

# Infrared signatures of hole and spin stripes in $\text{La}_{2-x}\text{Sr}_x\text{CuO}_4$

W.J. Padilla\* and M. Dumm†

*Department of Physics, University of California at San Diego, La Jolla, CA 92093-0319.*

Seiki Komiya and Yoichi Ando

*Central Research Institute of Electric Power Industry, Komae, Tokyo 201-8511, Japan.*

D. N. Basov

*Department of Physics, University of California at San Diego, La Jolla, CA 92093-0319.*

(Dated: November 11, 2018)

We investigate the hole and lattice dynamics in a prototypical high temperature superconducting system  $\text{La}_{2-x}\text{Sr}_x\text{CuO}_4$  using infrared spectroscopy. By exploring the anisotropy in the electronic response of  $\text{CuO}_2$  planes we show that our results support the notion of stripes. Nevertheless, charge ordering effects are not apparent in the phonon spectra. All crystals show only the expected infrared active modes for orthorhombic phases without evidence for additional peaks that may be indicative of static charge ordering. Strong electron-phonon interaction manifests itself through the Fano lineshape of several phonon modes. This analysis reveals anisotropic electron-phonon coupling across the phase diagram, including superconducting crystals. Due to the ubiquity of the  $\text{CuO}_2$  plane, these results may have implications for other high  $T_c$  superconductors.

The nature of spin and/or charge stripes in the cuprates and their involvement to high temperature superconductivity are currently at the center of a debate in condensed matter physics.[1] The expression “stripes” is a general term indicating that spins and/or holes may arrange themselves in quasi-one dimensional, or more complicated self-organized patterns. The stripe-ordered state minimizes the energy of holes doped in an antiferromagnetic matrix thus leading to new inhomogeneous state of matter.[2] Static one-dimensional (1D) charge stripes have been observed in the  $\text{La}_{2-x-y}\text{Nd}_y\text{Sr}_x\text{CuO}_4$  (LNSCO) system[3] with complimentary evidence from neutron and x-ray diffraction techniques. Although signatures of stripes by way of charge ordering have not been observed in  $\text{La}_{2-x}\text{Sr}_x\text{CuO}_4$  (LSCO) and other high temperature superconductors, there is evidence of the possible existence of dynamical stripes in these systems.[4] On the other hand, spin stripes have been discovered in LSCO[5] and many researchers agree upon their universality in high- $T_c$  superconductors. However a key issue regarding this new electronic state of matter concerns the role of stripes in relation to superconductivity, i.e. whether they are responsible for high temperature superconductivity or a competing phase with it.

Signatures of quasi one dimensional behavior should be observable in optical spectroscopy. In particular the lowering of symmetry due the formation of rigid charge density waves results is known to have dramatic implications for infrared (IR) active phonons.[6] Electronic 1D behavior can be directly probed by way of frequency dependent conductivity. An observation of the anisotropic conductivity in weakly doped LSCO is consistent with the notion of stripes [7, 8]. Notably these observations imply deviations from a hypothetical model in which the stripes are rigid rivers of charge embedded within an an-

tiferromagnetic background. Moreover, electronic and lattice fingerprints of 1D transport have not been systematically explored as a function of doping. The goal of this work is to apply infrared spectroscopy for the purpose of a detailed examination of spin/charge ordering effects in a series of well characterized LSCO crystals.

Infrared spectroscopy is a mature and powerful technique for the study of phonons[9, 10] electron-lattice coupling[11, 12] anharmonicity,[13] and charge and spin ordered states[6] resulting from a lowering of electronic and magnetic symmetry. Since precise measurements can be carried out with miniature single crystals, IR spectroscopy further permits a survey of the electronic anisotropy, which is naturally expected due the formation of stripes in cuprates. The inherent frequency dependent nature of IR spectroscopy coupled with temperature dependent measurements, allows one to determine characteristic energy scales associated with stripe formation as well as their T-dependence.

Here we present a systematic in-plane spectroscopic investigation on a series of detwinned ( $0 \leq x \leq 0.06$ ) single crystals and twinned ( $x = 0.08$ ) crystals of  $\text{La}_{2-x}\text{Sr}_x\text{CuO}_4$ , see Fig. 1. From the parent Mott insulator to the strontium doped superconducting samples ( $x = 0.06, 0.08$ ) the in plane electrodynamics are characterized by reflectance measurements using polarized light. Samples were coated *in situ* with gold or aluminum, and spectra measured from the coated surface were used as a reference. This method, discussed previously in detail,[14] allows one to reliably obtain the absolute value of the reflectance by minimizing the errors associated with non-specular reflection and small sample size. The optical conductivity  $\sigma_1(\omega) + i\sigma_2(\omega)$  and complex dielectric function  $\varepsilon_1(\omega) + i\varepsilon_2(\omega)$  was determined from a Kramers-Kronig (KK) transformation of the reflectance data after

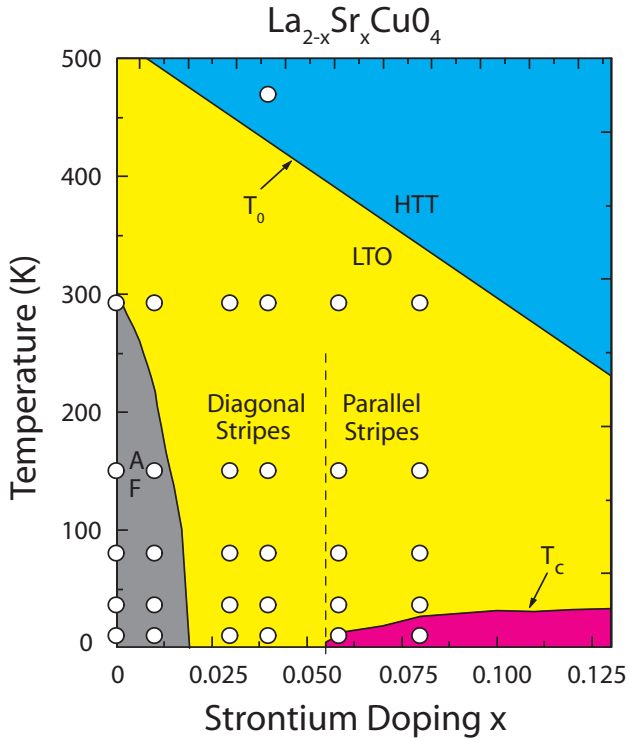


FIG. 1: Phase diagram of LSCO. Circles indicate samples and temperatures characterized in this study. AF refers to the long range 3D antiferromagnetic regime. The superconducting dome is indicated by the temperature  $T_c$ . The crystal structure  $\text{HTT} \rightarrow \text{LTO}$  is also noted.

extrapolation to low and high energies.[15] The samples are high quality single crystals grown by the travelling-solvent floating-zone technique,[16] and are cut into rectangular platelets with edges along the orthorhombic axes, (typical size of  $1.5 \times 0.5 \times 0.1 \text{ mm}^3$ ), where the c-axis is perpendicular to the platelets within an accuracy of  $1^\circ$ , as determined by x-ray Laue analysis.

One novelty of this study compared to existing results is the utilization of detwinned single crystals. Previous studies used ceramic samples or twinned crystals which make the results inconclusive or hard to interpret. The possibility to produce detwinned single crystals of LSCO has been known for over a decade.[17] However, well-detwinned LSCO crystals have become available only after the recent finding that twin structures in these materials can be observed on a polished ac-face under a microscope.[7, 18] Hence there has yet to be a systematic investigation of the in-plane anisotropy as a function of temperature. A common shortcoming of existing studies is the lack of observation of all of the theoretically expected phonons in the LTO (low temperature orthorhombic) phase of LSCO. Some infrared studies of LSCO have supposed the reason for this was due to the fact that the transition to orthorhombicity was small[19] and had negligible effects on phonon/electronic structure,

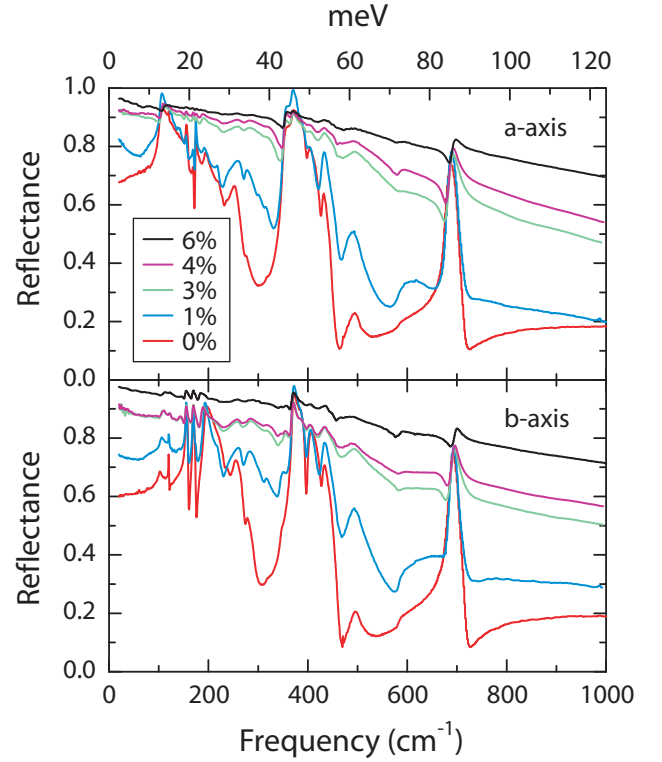


FIG. 2: Infrared region of the low temperature (10 K) reflectance for all detwinned crystals characterized. The a-axis spectra are displayed in the top panel and the b-axis results are shown in the bottom panel. The undoped parent compound (red curves) reveals its insulating character, and several IR active phonons can be observed in both axes. As carriers are added the reflectance background increases monotonically to larger values.

or that the presence of screening currents due to carriers obstructed their observation.[20] As will be shown, data for untwinned single crystals reported here allow us to remedy problems with earlier experiments.

It is instructive to discuss the phonon features of LSCO in the context of the evolution of the crystal structure as a function of temperature and doping. The phase diagram plotted in Fig. 1 is specific to LSCO, but many of the trends are generic for the Cuprates. LSCO has two distinct crystallographic phases, a high temperature tetragonal (HTT) phase, and a low temperature orthorhombic (LTO) phase. The separation between these two phases is denoted with the  $T_0$  line in Fig. 1. The undoped crystal  $\text{La}_2\text{CuO}_4$  ( $\text{La}214$ ) is a Mott insulator and exhibits long range 3D antiferromagnetism (AF). As holes are added to the system by substitution of  $\text{Sr}^{3+}$  for  $\text{La}^{2+}$ , the AF quickly dies off and a superconducting phase is found for dopings  $x \geq 0.055$ . The dashed vertical line in Fig. 1 indicates the region where stripes are known to undergo a  $45^\circ$  rotation.[21] The open circles indicate each doping and temperature characterized in this study.

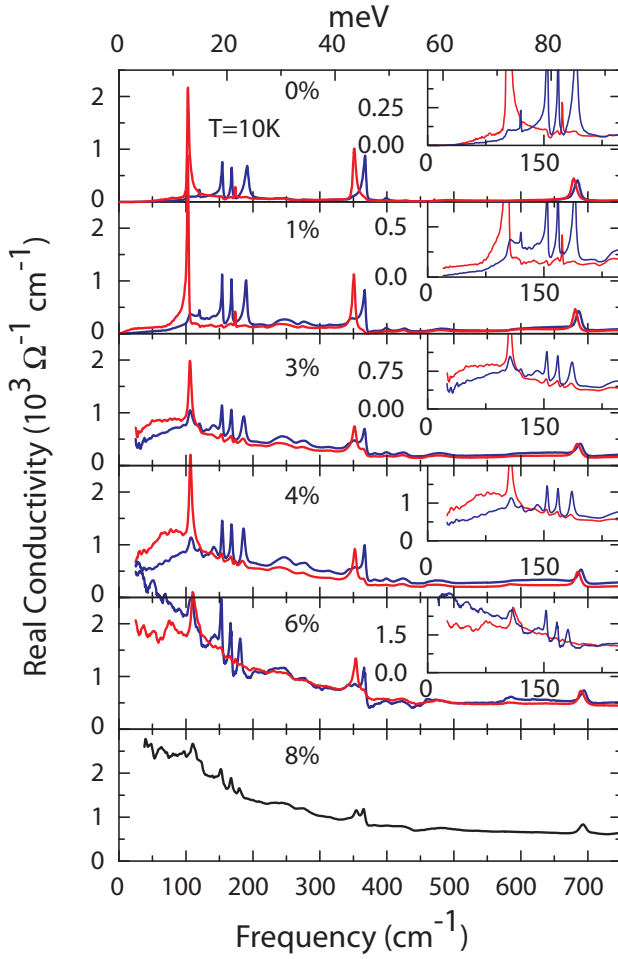


FIG. 3: The infrared portion of the real conductivity for undoped  $x=0.00$ , top panel, and  $x=0.01, 0.03, 0.04, 0.06$ , and  $0.08$  in the bottom panel. In the undoped compound (top) the a-axis data (red curves) display the expected four infrared active phonons and the b-axis spectra (blue curves) show the expected 7 IR active phonons. Insets detail the low frequency region and have the same horizontal and vertical units. All data are at  $T=10$  K.

Insights into the expected number of IR active phonon modes in the LSCO system are provided by point group theory. LSCO belongs to a family of structures related to the  $K_2NiF_4$  with space group  $I4/mmm$  (HTT) where the HTT phase can evolve into any of its Landau subgroups Bmab (LTO), Pccn (low-T tetragonal, LTT) and  $P42_1ncm$  (low-T orthorhombic 2, LTO-2).[22] In LSCO the  $HTT \rightarrow LTO$  transition is known to be of second order and occurs as a result from the bond length mismatch between the  $CuO_2$  planes and the  $La_2O_2$  bi-layers. This mismatch is relieved by a buckling of the  $CuO_2$  plane and a rotation of the  $CuO_6$  octahedra, (depicted in the lower panel Fig. 6), around the  $a_{ortho}$  axis which is the reason for the structural change. Additionally since the  $CuO_6$  octahedra are tilted along the longer  $b_{ortho}$  axis, a re-

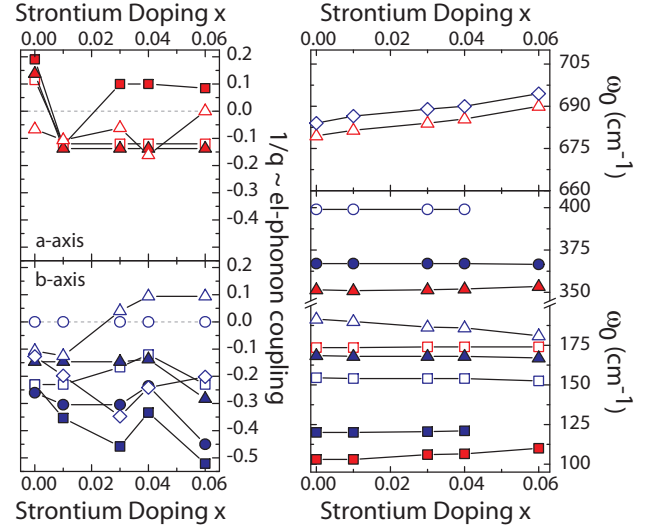


FIG. 4: Left panels: the doping dependence of the Fano parameter ( $1/q$ ) which is proportional to the electron phonon coupling, see text for a detailed description. Right panels: dependence of the center frequency of each IR active phonon vs. doping. The symbols in the right panel denoting each phonon may be used as a key for the left panel. All data are at  $T=10$  K.

duction of symmetry compared to the HTT phase occurs and group theory predicts 17 infrared active phonons,  $\Gamma_{IR} = 6B_{1u} + 4B_{2u} + 7B_{3u}$ , i.e. 7 modes along the b-axis, 4 modes along the a-axis and 6 along the c-axis. In contrast the HTT phase has  $\Gamma_{IR} = 3A_{2u} + 4E_u$ , 4 modes parallel to the ab-plane and 3 perpendicular to it. From this point on in the manuscript we drop the “ortho” subscript notation as all axes referred to will be the LTO phase unless otherwise indicated.

Fig. 2 displays the doping dependence of the reflectance  $[R(\omega)]$  at  $T=10$  K for both axes in the IR regime. In the undoped compound (red curves) relatively low values of  $R(\omega)$  reveal its insulating nature and oscillations, due to IR active phonons, are observable in both axes and in all dopings studied. As holes are added to the Cu-O plane the overall reflectance increases smoothly and monotonically. At 6% doping (black curves), all phonon modes are still observable, and the high  $R(\omega)$  values are indicative of metallic behavior.

In Fig. 3 we show the low temperature infrared portion of the frequency dependent real conductivity, calculated from a KK transformation of the data displayed in Fig. 2. In each panel the strontium doping is indicated, with the undoped parent compound La214 in the top panel and its superconducting counterparts  $x=6\%$ , ( $T_c=8K$ ) and  $x=8\%$ , ( $T_c=14K$ ) in the lower panels. The undoped parent compound exhibits low values of the conductivity consistent with its Mott insulating behavior. However the spectrum is punctuated by several strong phonons visible in both the a-axis and b-axis. As expected by

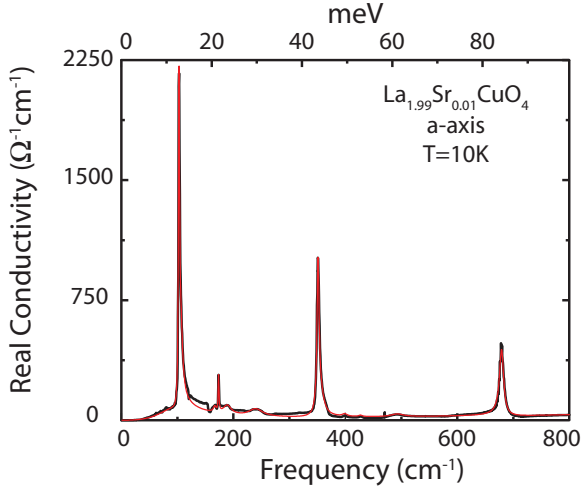


FIG. 5: Frequency dependent real conductivity  $\sigma_1(\omega)$  for 1% doped LSCO in the infrared regime (black curve). The coupling of the IR active phonons to an electronic continuum, evident here from their asymmetry, is visible for all 4 phonons. The red curve is a fit utilizing the Fano form for a resonance, listed in Eq. 1.

point group analysis we find 4 phonons in the a-axis data at 103, 173, 351, and 679  $\text{cm}^{-1}$  and 7 phonons in the b-axis conductivity at 120, 155, 168, 191, 367, 399, and 684  $\text{cm}^{-1}$ . The novelty of this result is that all phonons expected from group theory analysis can be identified in the spectra for detwinned samples. Moreover, the complete set of phonon peaks is also found in the data for twinned superconducting crystals  $x=0.08$  (bottom panel of Fig. 3).

We now turn to the analysis of the lineshape of phonon modes. Many resonances reveal an asymmetric line shape, (for an example see Fig. 5). It is instructive to quantify the degree of asymmetry through the so-called Fano analysis. We model the asymmetric features of the real conductivity using the form given in Equation 1,

$$\sigma_1 = \frac{S\omega}{4\pi} \left( \frac{(q\gamma + \omega - \omega_0)^2}{\gamma^2 + (\omega - \omega_0)^2} - 1 \right) \quad (1)$$

where,  $S$  is the strength of the oscillator,  $\gamma$  is the damping, and  $\omega_0$  is the center frequency of the phonon. An asymmetric phonon line shape is known to be related to electron-phonon coupling and is typically characterized through the Fano-Breit-Wigner (FBW) parameter  $q$ . The physical meaning of the parameter  $q$  is that it is inversely related to the strength of the interaction.[23] The asymmetric line shape is general and Fano derived a form for an oscillator coupled to an electronic continuum. These ideas were extended in ref.[11] to include the interaction with a number of discrete states with that of

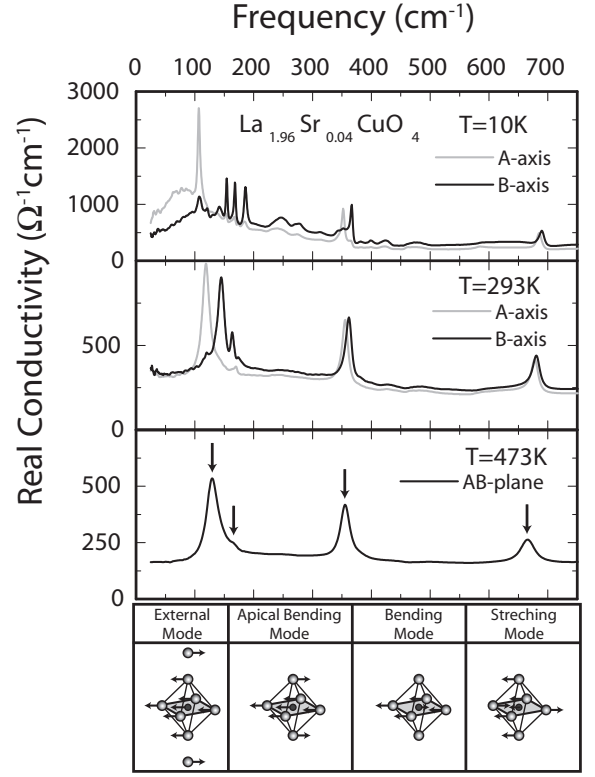


FIG. 6: Infrared region of  $\sigma_1(\omega)$   $\text{La}_{1.96}\text{Sr}_{0.04}\text{CuO}_4$  crystals at 10 K, room temperature, and in the HTT phase ( $T=473\text{K}$ ). The phonons for the HTT phase are indicated by arrows with the center frequencies given in the text. The bottom panel lists, in order from left to right, the assignment of each of these modes from low to high frequency as depicted by the  $\text{CuO}_6$  octahedra. The temperature evolution of these modes can be tracked into the LTO phase displayed in the top two panels. Both the a-axis (grey) and b-axis (black) data in the LTO phase are plotted.

a continua. The asymmetry in the line shape determines the energy range that the resonance is coupled. For example a line shape which dips on the low frequency (energy) side of the resonant frequency  $\omega_0$ , indicates the phonon is interacting with a continuum at higher energies, where the sign of  $1/q$  is positive in this case. For  $1/q=0$  a phonon assumes a symmetric lineshape and a Lorentz form is recovered.

In the left panels of Fig. 4 we quantify the degree of el-ph coupling, for both the a-axis and b-axis for and all dopings characterized at  $T=10\text{K}$  by plotting the doping dependence of  $1/q$  parameter in Eq. 1. For the undoped parent compound the  $1/q$  parameter for the a-axis phonons is positive for all modes with the exception of the 685  $\text{cm}^{-1}$  phonon. This result suggests that most of the a-axis modes interact with a continuum at higher energies whereas the 685  $\text{cm}^{-1}$  peak interacts with a continuum at lower energies. In contrast all b-axis phonons in  $\text{La}_{214}$  interact with a continuum at lower energies.[24] As carri-

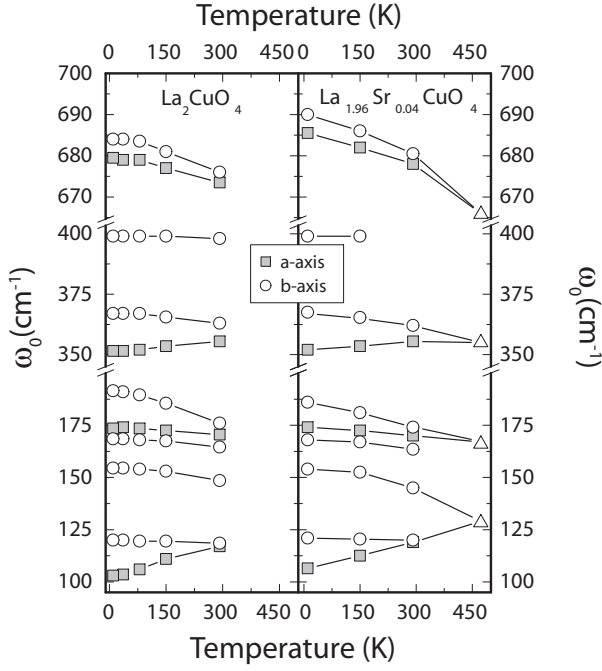


FIG. 7: Temperature dependence of the optically active phonons for undoped and 4% doped LSCO.

ers are introduced, at 1% doping we find an abrupt switch to negative  $1/q$  values for all a-axis phonons. The b-axis phonons in the  $x=0.01$  crystal do not show any anomalies. It should be noted that the 1% crystal is the only sample characterized in the AF regime, in which the spin lies perpendicular to the a-axis. The el-ph coupling relevant to the a-axis spectra is essentially doping independent throughout the rest of the underdoped regime of the phase diagram, with the exception of the lowest energy phonon which changes sign between 1% and 3%. The b-axis phonons however show significant signs of doping dependence and their  $1/q$  values are roughly 2-3 times greater than those in the a-axis. Lastly we notice that the values for  $1/q$  in the 6% superconducting sample are similar to those crystals which do not exhibit SC.

Let us examine directly the HTT to LTO transition through the spectra of the real conductivity. In Fig. 6 the infrared region of  $\text{La}_{1.96}\text{Sr}_{0.04}\text{CuO}_4$  at 10K, and 292K along with the spectrum from the HTT phase ( $T=473\text{K}$ ) is shown. The HTT phase, as stated above, has four in-plane infrared active phonons and their normal modes are depicted in the lower portion of Fig. 6, while in the panel above, each mode is indicated by an arrow with their corresponding center frequencies at 129, 165, 355, 666  $\text{cm}^{-1}$ . It can be seen that some of these modes in the HTT phase split nearly symmetrically from their location into phonons in the a-axis and b-axis of the LTO phase. For example the phonon at 355  $\text{cm}^{-1}$  splits into the 352  $\text{cm}^{-1}$  and 367  $\text{cm}^{-1}$  phonons in the a-axis and b-axis

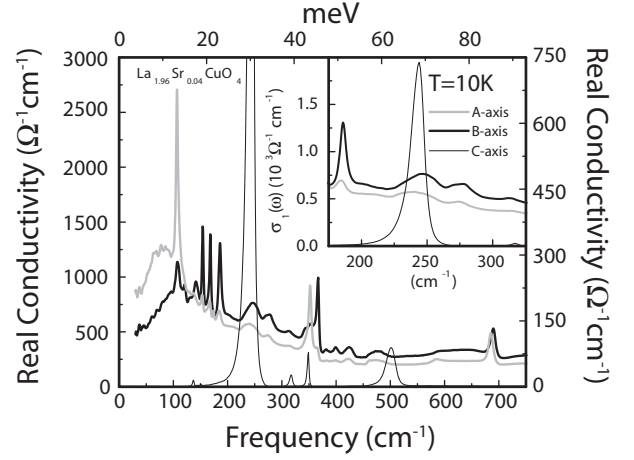


FIG. 8: Low temperature infrared spectra measured for polarization of  $\mathbf{E}$  vector along of all three crystallographic axes for the LTO phase of  $x=4\%$  Sr doped LSCO. The a-axis and b-axis spectra (thick gray and thick black lines respectively) are shown in the main panel and their units correspond to the left coordinate. In order to display all phonons, the c-axis conductivity (thin black line) has been multiplied by a factor of 4 (right coordinate). The inset shows the c-axis phonon at 244  $\text{cm}^{-1}$  and the a-axis and b-axis all on the same vertical scale.

respectively. The high frequency phonon at 666  $\text{cm}^{-1}$  hardens and splits into the phonons at 680  $\text{cm}^{-1}$  (a-axis) and 684  $\text{cm}^{-1}$  (b-axis). The splitting is such that the a-axis phonon always lies lower in frequency compared to the b-axis phonon in all dopings and temperature ranges characterized, (also see the right pane of Fig. 7).

In Fig. 7 we show the temperature dependence of the center frequencies of all in-plane phonons for both the parent Mott-Hubbard insulator and for 4% LSCO. Many phonons are seen to be temperature independent with a few exceptions. The lowest frequency a-axis phonon at 120  $\text{cm}^{-1}$  is seen to soften with decreasing temperature by nearly 15  $\text{cm}^{-1}$ , while the b-axis phonon at 176  $\text{cm}^{-1}$  hardens by the same amount. Phonons from the a and b-axis of the HTT bending mode at 355  $\text{cm}^{-1}$  split symmetrically and soften and harden, respectively, by 4  $\text{cm}^{-1}$  with the a-axis phonon lying lower in frequency. The high frequency a-axis and b-axis phonons from the HTT stretch mode are seen to harden by about 7  $\text{cm}^{-1}$ . Interestingly they also exhibit a significant doping dependence, as they both harden by 10  $\text{cm}^{-1}$  from undoped compound to the superconducting 6% sample.

For completeness, we also show in Fig. 8 the c-axis data obtained for the  $x=4\%$  LSCO crystal along with the a-axis and b-axis spectra, all at 10 K. As previously mentioned one would expect 6 IR active modes in the c-axis in the LTO phase. In accord with this expectation we find phonons at 137, 151, 244, 317, 349, 501  $\text{cm}^{-1}$ . With this full characterization of lattice modes along all

crystallographic orthorhombic axes, we can understand the origin of additional features seen for the in-plane measurements. For example the structure near  $250\text{ cm}^{-1}$  and  $500\text{ cm}^{-1}$  in both the a-axis and b-axis spectra is likely to originate from the mixture of the c-axis polarization. This unwanted effect is likely to be connected with roughness of the surface and/or minor miss-cut of the sample surface.[25] One can also observe unwanted leakage from the a-axis to the b-axis and vice versa, i.e. the triplet of phonons centered near  $170\text{ cm}^{-1}$  in the b-axis can be seen in the a-axis data.

Let us now examine the anisotropy of the electronic background in the infrared conductivity data depicted in Fig. 3. As holes are added to the system by increasing the strontium doping the conductivity increases and evolves smoothly and monotonically in both axes. We find that the electronic background shows substantial anisotropy in all untwinned samples with dopings  $x < 6\%$ .[26] This is in accord with transport measurements on detwinned single crystals of LSCO.[7] Enhancement of the conductivity occurs along the spin stripe direction (a-axis). This finding is therefore consistent with the notion of inherently conducting stripes. We also note that the anisotropy is greatest in the 1% crystal and is suppressed with the increasing doping. This result supports the relevance of spin stripes for the electronic transport in LSCO. Indeed, the separation between the stripes is enhanced at low dopings [4] which inevitably should reduce the conductivity across the stripe direction.

We have shown a detailed temperature and doping dependent systematic investigation of the electromagnetic properties of the underdoped region of LSCO. The observation of all expected IR active modes as predicted by group theory indicates the quality of the samples studied here. It was found that all crystals exhibit lineshapes suggestive of electron-phonon coupling. No anomalies in the electron-phonon coupling are found near 5 % doping where the onset of superconductivity occurs in the phase diagram of LSCO. It is therefore safe to conclude that the superconducting phase boundary near  $x=5\%$  is unrelated to modifications of the interaction between the doped holes and the lattice.

Electronic anisotropy evident in Fig. 3 supports the notion of stripes. For example in all detwinned crystals, the low temperature low frequency limit of  $\sigma_1(\omega)$  shows that the a-axis has larger values supporting the suggestion that stripes are inherently conducting. The analysis of the phonon line shape calculated in the left panels of Fig. 4 shows stronger electron phonon coupling along the b-axis compared to the a-axis. This in-plane el-ph anisotropy also supports the notion of stripes. The orthorhombicity in these systems was shown to be small and not sufficient to account for the values calculated here. Thus despite the two-dimensional nature of the layered  $\text{CuO}_2$  planes, both the electronic conductivity and phonon line shape anisotropy are consistent with one-

dimensional behavior and therefore support the notion of stripes.

The spectra of IR active phonons detailed in Fig. 3 show that all expected modes evolve smoothly and continuously as carriers are added to the system. This can be seen directly in the right panels of Fig. 4. Further the temperature dependence of the phonons vs. temperature (Fig. 7) shows a continuous evolution. It must be noted that there are no indications of new phonon modes anywhere in the underdoped region of the phase diagram. Also the temperature and doping dependent evolution is linear with no signs of anharmonic behavior. Since the lowering of crystal symmetry due to the formation of charge density waves results in a change in the number of IR modes and/or anharmonic behavior, the findings presented above rule this out. This result is inconsistent with the notion of static charge ordering associated with spin stripes in LSCO. It is yet to be seen if the hypothesis of fluctuating stripes can account for our observations. As the  $\text{CuO}_2$  plane is a common element to many high  $T_c$  superconductors, these results may be important and more general than just limited to LSCO.

This research was supported by the U.S. Department of Energy Grant No. DE-FG03-00ER45799.

---

\* present address: Los Alamos National Laboratory, MS K764 MST-10, Los Alamos NM 87545; Electronic address: willie@lanl.gov

† present address: 1. Physikalisches Institut, Universität Stuttgart, 70550 Stuttgart, Germany

- [1] V.J. Emery, S.A. Kivelson, J.M. Tranquada, Proc. Natl. Acad. Sci. USA **96** 8814-8817 (1999).
- [2] Review chapter to appear in *The Physics of Conventional and Unconventional Superconductors* edited by K. H. Bennemann and J.B. Ketterson (Springer-Verlag) by E.W. Carlson, V.J. Emery, S. A. Kivelson, D. Orgad.
- [3] J.M. Tranquada, B.J. Sternlieb, J.D. Axe, Y. Nakamura, S. Uchida, Nature **375**, 561 (1995).
- [4] K. Yamada, C.H. Lee, K. Kurahashi, J. Wada, S. Wakimoto, S. Ueki, H. Kimura, Y. Endoh, S. Hosoya, G. Shirane, R. J. Birgeneau, M. Greven, M.A. Kastner, Y.J. Kim, Phys. Rev. B **57**, 6165 (1998).
- [5] S-W. Cheong, *et al.*, Phys. Rev. Lett. **67**, 1791 (1991); T. E. Mason, *et al.*, Phys. Rev. Lett. **68**, 1414 (1992); T. R. Thurston, *et al.*, Phys. Rev. B **46**, 9128 (1992); K. Yamada, *et al.*, Phys. Rev. Lett. **75**, 1626 (1995).
- [6] G. Grüner, Density Waves in Solids (Addison-Wesley, Reading, MA, 1994).
- [7] Y. Ando, K. Segawa, S. Komiya, A.N. Lavrov, Phys. Rev. Lett. **88**, 137005 (2002).
- [8] M. Dumm, Seiki Komiya, Yoichi Ando, D.N. Basov, Phys. Rev. Lett. **91**, 077004 (2003).
- [9] A. Damascelli, K. Schulte, D. van der Marel, A.A. Menovsky, Phys. Rev. B **55**, R4863 (1997).
- [10] W.J. Padilla, D. Mandrus, D.N. Basov, Phys. Rev. B **66**, 035120 (2002).
- [11] L.C. Davis and L.A. Feldkamp, Phys. Rev. B **15**, 2961

- (1977).
- [12] S. Lupi, M. Capizzi, P. Calvani, R. Ruzicka, P. Maselli, P. Dore, and A. Paolone, *Phys. Rev. B* **57**, 1248 (1998).
  - [13] R.A. Cowley, *Rep. Prog. Phys.* **31**, 123 (1968).
  - [14] C. Homes, M.A. Reedyk, D.A. Crandels, and T. Timusk, *Appl. Opt.* **32**, 2976 (1993).
  - [15] F. Wooten, *Optical Properties of Solids* (Academic Press, New York, 1972).
  - [16] Y. Ando, A.N. Lavrov, S. Komiya, K. Segawa, and X.F. Sun, *Phys. Rev. Lett.* **87**, 017001 (2001).
  - [17] T. Thio, C.Y. Chen, B.S. Freer, D.R. Gabbe, H.P. Jenssen, M.A. Kastner, P.J. Picone, N.W. Preyer, R.J. Birgeneau, *Phys. Rev. B* **41**, 231 (1990).
  - [18] A. N. Lavrov, S. Komiya, Y. Ando, *Nature* **418**, 385 (2002).
  - [19] S. Tajima, T. Ido, S. Ishibashi, T. Itoh, H. Eisaki, Y. Mizuo, T. Arima, H. Takagi, and S. Uchida, *Phys. Rev. B* **43**, 10496 (1991).
  - [20] A. P. Litvinchuck, C. Thomson, and M. Cardona, in *Physical Properties of High-Temperature Superconductors IV*, edited by D.M. Ginsberg (World Scientific, Singapore, 1994).
  - [21] M. Matsuda, M. Fujita, K. Yamada, R.J. Birgeneau, M.A. Kastner, H. Hiraka, Y. Endoh, S. Wakimoto, G. Shirane, *Phys. Rev. B* **62**, 9148 (2000).
  - [22] J.D. Axe, A.H. Moudden, D. Hohlwein, D.E. Cox, K.M. Mohanty, A.R. Moodenbaugh, Youwen Xu, *Phys. Rev. Lett.* **62**, 2751 (1989).
  - [23] U. Fano, *Phys. Rev.* **124**, 1866 (1961).
  - [24] The phonon in the b-axis located near  $400\text{cm}^{-1}$  has a small oscillator strength which makes the determination of the FBW constant arbitrary. Thus the asymmetric analysis has not been carried out for this phonon, as indicated by a  $1/q=0$ , i.e. a Lorentzian lineshape.
  - [25] S. Tajima, S. Uchida, D. van der Marel, D. N. Basov, *Phys. Rev. Lett.* **91**, 129701 (2003).
  - [26] This trend is reversed in the  $x = 6\%$  sample for which the b-axis conductivity is enhanced (bottom of Fig. 3). One caveat known from neutron measurements is that spin stripes undergo a  $45^\circ$  rotation at a strontium doping of  $x = 5.5\%$ , above which the stripes lie parallel to the Cu-O bond direction, for example see ref. [21]. Moreover, single crystals near  $x=5.5-6\%$  doping commonly reveal the coexistence of diagonal and collinear stripes. It is likely that the anisotropic anomaly we find in the  $x=6\%$  crystal may be related to complications resulted from the coexistence of the two forms of spin stripe patterns.